Colloids and Surfaces A: Physicochem. Eng. Aspects 534 (2017) 105–111

Contents lists available at ScienceDirect

Colloids and Surfaces A: Physicochemical and Engineering Aspects

journal homepage: www.elsevier.com/locate/colsurfa

Dynamics of a flexible fibre in a sheared two-dimensional foam: Numerical simulations

Vincent J. Langlois [a,*], Stefan Hutzler [b]

[a] Laboratoire de Géologie de Lyon, Université Claude Bernard Lyon 1 – ENS de Lyon – CNRS, 2 rue R. Dubois, 69100 Villeurbanne, France
[b] School of Physics, Trinity College Dublin, The University of Dublin, Ireland

HIGHLIGHTS

- We propose a novel model for the dynamics of flexible fibres within a flowing foam.
- As in a Newtonian fluid fibres experience a tumbling instability.
- The complex motion of bubbles does not allow fibres to align with the flow.

GRAPHICAL ABSTRACT

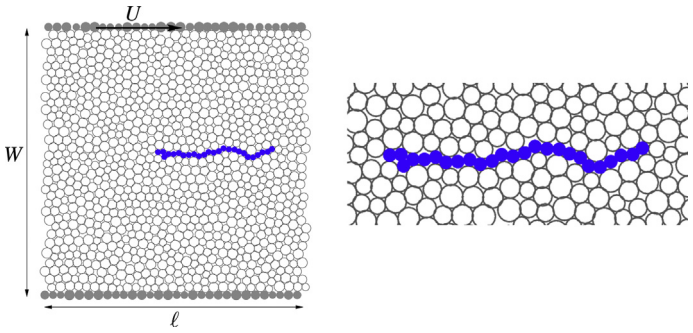

ARTICLE INFO

Article history:
Received 1 December 2016
Received in revised form 22 February 2017
Accepted 27 February 2017
Available online 6 March 2017

Keywords:
Fibre-laden foams
Papermaking
Tumbling instability
Bubble model

ABSTRACT

Recently there has been a renewed interest in using foamy suspensions of wood fibres as a carrier fluid in papermaking but there is a lack of fundamental understanding of the dynamics of such a three-phase system. In this article we propose a numerical model for the dynamics of an individual flexible fibre within a flowing foam, based on discrete-element methods. As is observed in a Newtonian shear flow, we observe that the fibre systematically experiences a tumbling instability: the disordered motion of bubbles cannot prevent the pseudo-periodical flip of the fibre. Our simulations show that the tumbling time decreases almost as the inverse of the strain rate. It also decays when the fibre length is increased, asymptoting to a finite constant. The tumbling time is found to be independent of the stiffness of the fibre. Because of their tumbling motion, long and flexible fibres spend most of the time in a coiled geometry. This would imply that using foam as a carrier fluid is not enough to keep fibres aligned with the flow. However, further refinements of the model will need to be considered to arrive at firm conclusions regarding alignment.

1. Introduction

The possibility of replacing water by a liquid foam as the carrier fluid for wood fibres in papermaking has led to a renewed interest in the technique by the paper industry. Although this idea was initially proposed in the 1970s [22], quantitative investigations of the behaviour of fibre-laden foams have only begun quite recently. The use of a fibre-laden foam would considerably reduce the water consumption and consequently the energy needed for the drying of the paper. Furthermore, the technique might enable improvement and better control of the properties of the final fibre network: the same method could then be applied to the manufacturing of other novel fibrous materials (e.g. for insulation, non-woven textiles, oil absorption, etc.).

* Corresponding author.
E-mail address: vincent.langlois@univ-lyon1.fr (V.J. Langlois).

http://dx.doi.org/10.1016/j.colsurfa.2017.02.089
0927-7757/

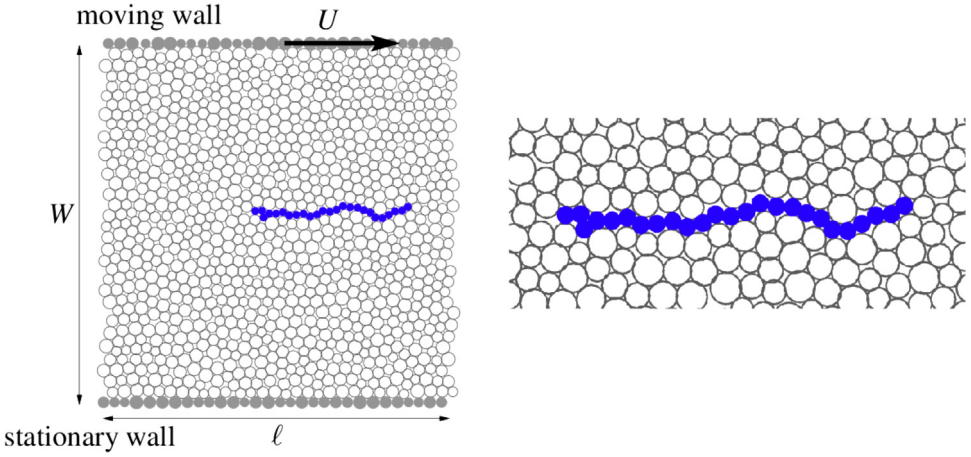

Fig. 1. Foam produced by the bubble model, containing a fibre represented by 25 connected disks (appearing in blue), and close-up view of this fibre surrounded by bubbles. Fixed streamwise velocities (0 and U, respectively) are imposed on the bubbles composing both side-walls (full grey). Note that in the actual simulations the length of the cell is much longer (ℓ about 100 bubble diameters).

In the papermaking framework, several experimental studies [2,3,11,10] have recently investigated the influence of the fibres (depending on their physico-chemical characteristics) on the properties of the wet foam used as carrier fluid: incorporating fibres while mixing the foaming liquid produces a foam with smaller bubbles and a higher liquid fraction than without fibres. Foam viscosity has been found to increase with increased content of rough wood fibres, although the foam still remains shear-thinning. This viscosity increase might not occur when using artificial smooth fibres such as viscose. Further work also addressed the alteration of local foam geometry in the presence of fibres and the slow-down in foam coarsening [27]. The influence of the foam on the properties of the final dry fibre network has been studied by Al-Qararah et al. [1], who showed that the pore size distribution in the paper sheet is more regular if the fibres are deposited from a foam suspension, rather than from classical water-based pulp.

It is important to investigate theoretically and numerically the dynamics of fibre-laden foams, in order to better understand the key parameters that control the interactions between fibres and bubbles: how does the presence of fibres affect the properties of the foam, and how can we use the foam carrier in order to tune the properties of the final fibre network?

In the past 20 years, the physics of liquid foams has known flourishing progress [26,5], whether it deals with the physico-chemical properties of the thin liquid films, the quasi-static properties of a foam (bubble coarsening and ripening, drainage) or its dynamical behaviour (influence of flow on topology, rheology). Also, since the pioneering theoretical works of Jeffery [12] on the dynamics of ellipsoidal particles, the study of fibres in Newtonian fluid flows has been the subject of many experimental and numerical studies, with motivations as diverse as papermaking, water purification, dynamics of DNA molecules or microswimmers [8,29,18,24,23,9,16,25,15,7]. In particular, fibre suspensions have often been modelled by studying the interactions between a laminar simple shear or Poiseuille flow and flexible rods modelled as strings of spherical (or circular) beads.

Here we propose to combine such a model for fibres with a model that describes a foam itself as a packing of soft spheres or disks (in 2D). This so-called bubble model, or soft-sphere model was introduced by Durian [6] in order to simulate mechanical properties of wet foams. As shown by Langlois et al. [14], this simplistic but computationally efficient approach is sufficient to reproduce the basic features of the rheology of foams: existence of a yield stress, Herschel–Bulkley shear-thinning rheology, occurrence of shear-bands in a Hele-Shaw cell, and it can also be appropriate for more complex geometries [13].

In this article we will consider the behaviour of a single fibre in a two-dimensional (2D) foam under shear, as a preliminary study in order for further investigations of the rheology of three-dimensional fibre-laden foams. The article is organized as follows: in Section 2 we describe the implementation of the bubble model and the modelling of the fibres; in Section 3 we analyze the motion of the fibre as a function of its length and stiffness, strain rate and channel width. Finally we draw conclusions regarding the use of foam as a carrier fluid for fibres.

2. Numerical model

2.1. Bubble model

The 2D foam, as described by the bubble model [6,14], is a dense packing of circular bubbles. A small polydispersity in bubble size is introduced to prevent crystallization of the bubbles, with each bubble radius R_i being chosen within a uniform distribution bounded by $R_0 \times (1 \pm 0.2)$, R_0 being the average radius. The foam is produced by compressing a sample of 2000–10,000 bubbles between two side-walls, of length ℓ=200 R_0 and made of fixed bubbles. The final state is obtained for a gap W between these walls (see Fig. 1), defined by the packing fraction $\sum \pi {R_i}^2/(W\ell)$ =0.90 (the overlaps between bubbles being neglected). This corresponds to an effective liquid fraction ϕ = 0.10. One of the side-walls is then moved tangentially at a constant speed U, which defines the average strain rate as $\dot{\gamma} = U/W$. The other side-wall is kept stationary. The dynamics of the foam are computed by solving Newton's second law for each individual bubble, using classical numerical techniques originally developed for Molecular Dynamics [17]. Periodic boundary conditions are applied in the streamwise direction.

Bubbles interact with one another through elastic and viscous forces. When overlapping, two bubbles i and j, located respectively at $\mathbf{r}_i$ and $\mathbf{r}_j$ and of radii R_i and R_j, repel each other via a linear elastic force. A bubble j then exerts on bubble i the force

$$\mathrm{F_r}^{ij} = -\kappa \frac{2R_0}{R_i + R_j} \Delta_{ij} \mathbf{n}_{ij}. \quad (1)$$

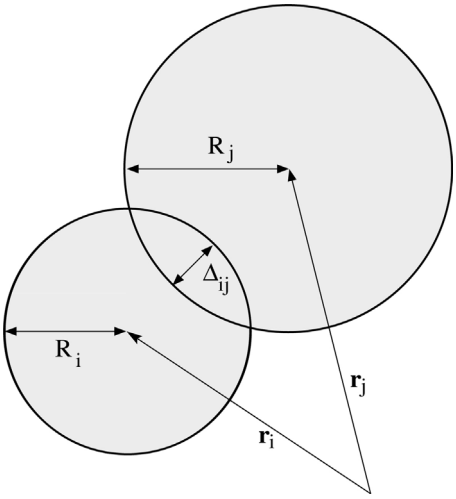

Fig. 2. Overlap Δ_{ij} between two contacting bubbles of radii R_i and R_j, located at $\mathbf{r}_i$ and $\mathbf{r}_j$, respectively.

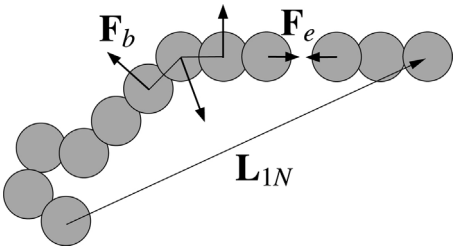

Fig. 3. Elastic ($\mathbf{F}_e$) and bending ($\mathbf{F}_b$) forces experienced by the disks representing the fibre, whose shape is characterized by its end-to-end vector. Elastic forces tend to bring the fibre length back to equilibrium and bending forces tend to keep the fibre straightened.

where κ is the coefficient of elasticity (related to surface tension), $\mathbf{n}_{ij}$ is the unit normal vector between bubbles i and j, defined by

$$\mathbf{n}_{ij} = \frac{\mathbf{r}_j - \mathbf{r}_i}{|\mathbf{r}_j - \mathbf{r}_i|}, \tag{2}$$

and the overlap Δ_{ij} (see Fig. 2) is given by $\Delta_{ij} = (R_i + R_j) - |\mathbf{r}_j - \mathbf{r}_i|$. The ratio $2R_0/(R_i + R_j)$ in Eq. (1) takes into account that larger bubbles are easier to deform than smaller ones. In a real flowing foam, energy is dissipated by the viscosity of the liquid within the films between bubbles. This is accounted for in the bubble model by introducing a viscous force $\mathbf{F}_v$ acting on a bubble i in contact with a bubble j:

$$\mathbf{F}_v{}^{ij} = c_b(\mathbf{v}_j - \mathbf{v}_i) \tag{3}$$

where c_b is a dissipation constant and $\mathbf{v}_i$ and $\mathbf{v}_j$ are the respective bubble velocities.

The two forces $\mathbf{F}_r{}^{ij}$ and $\mathbf{F}_v{}^{ij}$ allow us to define the dimensionless Deborah number $\mathrm{De} = \dot{\gamma} c_b/\kappa$, that relates the timescale of bubble dynamics $\tau_b = c_b/\kappa$ to the shear timescale $1/\dot{\gamma}$.

2.2. Particle model of the fibre

Following the seminal works of Yamamoto and Matsuoka [28], we model a deformable fibre as a string of N disks of radius $R_f = 0.6R_0$. This model is particularly appropriate within the bubble model, since the dynamics of these fibre particles can be computed together with the dynamics of the bubbles. Within the fibre, each particle exerts both an elastic and a bending force on its neighbours (see Fig. 3). Elasticity is modelled by adding linear springs between each pair of adjacent fibre particles. The elastic force experienced by a fibre particle i is then

$$\mathbf{F}_e{}^i = -\kappa(l_i - l_0)\,\mathbf{n}_{i-1,i} + \kappa(l_{i+1} - l_0)\,\mathbf{n}_{i,i+1} \tag{4}$$

with $l_i = |\mathbf{r}_i - \mathbf{r}_{i-1}|$ and $l_0 = 1.8\,R_f$ the distance between two fibre particles at equilibrium. This force tends to bring the fibre back to its equilibrium length $L_0 = (N-1)l_0$. Discretizing the bending free energy of a continuous elastic rod gives the following expression for the bending force acting on the particle i [9,20]:

$$\begin{aligned}\mathbf{F}_b^i = S \times \kappa R_0 \times \Bigg\{ & \frac{\epsilon_{i-1}}{l_i}\,\mathbf{n}_{i-2,i-1} - \left[\frac{\epsilon_{i-1}}{l_i}\,\mathbf{n}_{i-2,i-1}\cdot\mathbf{n}_{i-1,i} + \frac{\epsilon_i}{l_{i+1}} \right. \\ & \left. + \frac{\epsilon_i}{l_i}\,\mathbf{n}_{i-1,i}\cdot\mathbf{n}_{i,i+1} \right] \mathbf{n}_{i-1,i} + \left[\frac{\epsilon_i}{l_{i+1}}\,\mathbf{n}_{i-1,i}\cdot\mathbf{n}_{i,i+1} + \frac{\epsilon_i}{l_i} \right. \\ & \left. + \frac{\epsilon_{i+1}}{l_{i+1}}\,\mathbf{n}_{i,i+1}\cdot\mathbf{n}_{i+1,i+2} \right] \mathbf{n}_{i,i+1} - \frac{\epsilon_{i+1}}{l_{i+1}}\,\mathbf{n}_{i+1,i+2} \Bigg\}\end{aligned} \tag{5}$$

with $\epsilon_i = l_0$ if $2 \le i \le N-1$ and $\epsilon_i = 0$ for $i = 1$ or N. This force tends to restore alignment of each triplet of adjacent fibre particles, and therefore straightens the fibre. The parameter S represents the dimensionless stiffness of the fibre. Finally, the interaction between a fibre particle and a bubble, or between two non-adjacent fibre particles, is treated as if it were a bubble-bubble interaction (with repulsive and dissipative forces, see Eqs. (1) and (3)). We will return to this treatment in Section 4 where we discuss the modelling of fibre roughness.

In order to describe the shape of the fibre during the dynamics, we define its end-to-end vector $\mathbf{L}_{1N}$ (as illustrated in Fig. 3), whose normalized components are noted as

$$\Delta x(t) = \frac{x_N(t) - x_1(t)}{L_0} \quad \text{and} \quad \Delta y(t) = \frac{y_N(t) - y_1(t)}{L_0} \tag{6}$$

where the indices 1 and N correspond to both ends of the fibre. For instance, when the fibre is perfectly aligned in the streamwise x-direction, we have $\Delta y = 0$, and if it is neither stretched nor compressed, $\Delta x = 1$. Following Słowicka et al. [21], we also define the fractional compression of the fibre as

$$\alpha(t) = 1 - \frac{L(t)}{(N-1)l_0} \tag{7}$$

with $L(t) = |\mathbf{L}_{1N}|$ the absolute distance between the two ends of the fibre. α can be seen as a measurement of the state of the coiling of the fibre. When the fibre is coiled, we have $\alpha > 0$, whereas at equilibrium $\alpha = 0$ and when the fibre is stretched $\alpha < 0$.

2.3. Time integration

At a given iteration, all forces acting on each bubble/particle are computed. Overlaps between bubbles are found by using the linked cell algorithm [17]. As in previous implementations of the model [14,19,13], an effective mass is assigned to each bubble/particle and we use the Verlet algorithm (of fourth order of precision) [17] to compute the position of each bubble/particle at the next iteration from Newton's second law. The mass is chosen so that the motion of each bubble remains overdamped and inertia is therefore negligible in the dynamics: we set the ratio $\kappa m_b/{c_b}^2 = 1.5 \times 10^{-2}$. In order to compute accurately each collision between bubbles, the iterative timestep Δt is chosen 100 times smaller than the characteristic viscous timescale:

$$\Delta t = \frac{\tau_b}{100} \quad with \quad \tau_b = \frac{m_b}{c_b} \tag{8}$$

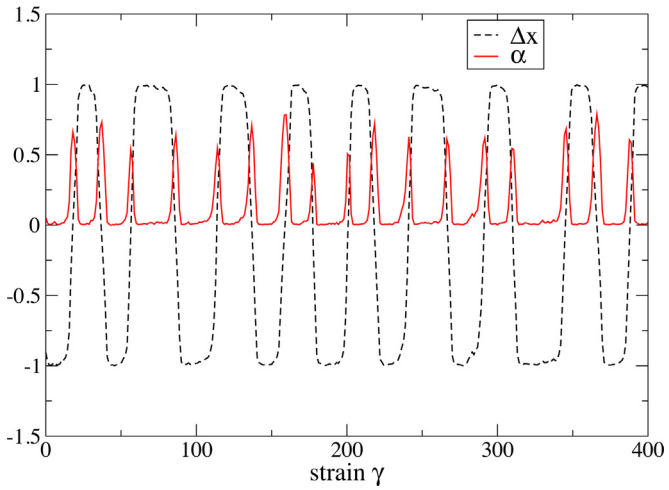

Fig. 4. Normalized streamwise component $\Delta x/l_0$ of the end-to-end vector and fractional compression of the fibre as a function of strain, for $N = 50$, $S = 1.0$ and $\mathrm{De} = 1.0 \times 10^{-3}$. Most of the time the fibre is undeformed and oriented along the streamwise direction. Each peak in α corresponds to the fibre flipping (which results in reversing its direction).

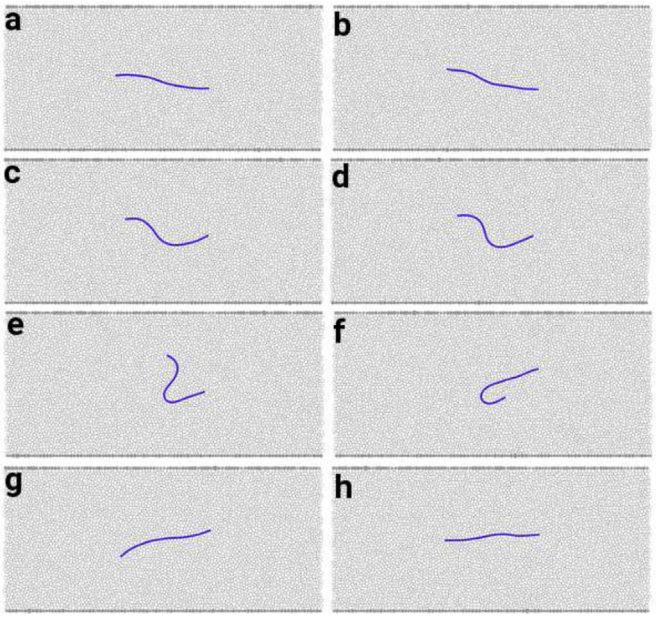

Fig. 5. Successive snapshots of a fibre of length $N = 50$ undergoing a 'flip'. The x-position of the middle particle of the fibre is kept fixed in this representation. Images are separated by $\Delta\gamma = 2$.

3. Dynamics of a fibre in a shear flow

3.1. Tumbling instability

Let us first remark that the presence of a single fibre does not affect the average linear velocity profile in the gap. We plot in Fig. 4 the streamwise extension Δx of the fibre as a function of strain $\gamma = \dot{\gamma} \times t$, for a length $N = 50$, a strain rate $\mathrm{De} = 1.0 \times 10^{-3}$ and a stiffness $S = 1.0$. In this example, we can observe that the fibre spends most of the time in a straight configuration ($|\Delta x| \simeq 1$ and $\alpha \simeq 0$), during which it is roughly aligned with the direction of the flow. However, it also experiences successive flips, during which it rapidly coils ($\alpha > 0.5$) before straightening again in the opposite direction. This tumbling motion, which is also observed for an individual fibre within a viscous Newtonian flow [20,21], appears to be roughly periodic. Hence, the presence of the bubbles is not sufficient to channel the motion of fibre and prevent this instability. The snapshots in Fig. 5 illustrates the successive shapes taken by the fibre during one of these flips.

3.2. Dependence on strain rate

A fibre flip is identified by the rapid change in sign of Δx and we mark its occurrence in time when $\Delta x = 0$. The duration between two consecutive flips defines the tumbling time T_t. The average tumbling time for a given strain rate is computed over at least 50 flip events. Different from the case of a viscous shear flow in a Newtonian fluid, it is possible in a foam to define an internal timescale, independently of the strain rate. We therefore rescale the tumbling time with the internal timescale τ_b, while varying the strain rate $\dot{\gamma}$ between $\mathrm{De} = 5 \times 10^{-5}$ and $\mathrm{De} = 1 \times 10^{-2}$. It has been shown that the bubble model represents accurately the Herschel–Bulkley rheology: $\tau = \tau_y + A \times \dot{\gamma}^{1/2}$ over this range [14]. If we keep the length and stiffness of the fibre fixed, respectively $N = 50$ and $S = 1$, we observe the variation shown in Fig. 6. As theoretically predicted by Jeffery [12] for rigid ellipsoids and numerically observed by Jeffery [28] for rigid particulate rods in a Newtonian shear flow, we observe that the tumbling time decreases when $\dot{\gamma}$ or De increase. However, the above studies predict that the tumbling time scales

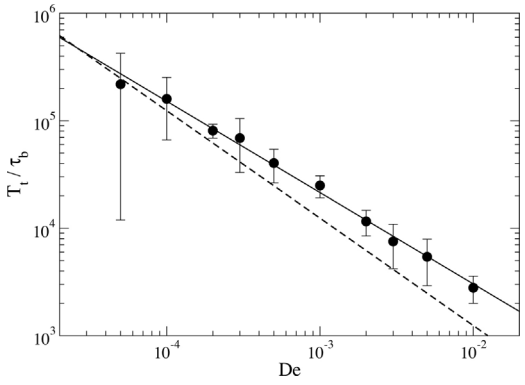

Fig. 6. Tumbling time as a function of the dimensionless strain rate De, for a fibre of length $N = 50$ and stiffness $S = 1$. The solid line represents the best fit by a power law (see Eq. (9)). The dashed line represents the best fit by an inverse function: $T_t/\tau_b = 12.4 \times \mathrm{De}^{-1}$.

linearly with the inverse strain rate $\dot{\gamma}^{-1}$. In the case of a foam flow, the best fit to our data to a power law results in

$$\frac{T_t}{\tau_b} = 60.4 \times \mathrm{De}^{-0.85 \pm 0.03} \tag{9}$$

which departs only slightly from the prediction (exponent -1) for slender objects.

3.3. Influence of fibre length

Since the scaling of the tumbling time with the strain rate is close to an inverse relationship, we now define the dimensionless tumbling time as $\tau_t = \dot{\gamma} \times T_t$. In Fig. 7, we plot this rescaled tumbling time as a function of the fibre length, all other parameters being kept constant. As can be observed, the longer the fibre, the faster it tumbles, which differs from results obtained by Yamamoto and Matsuoka [28] for rigid fibers in the viscous shear flow of a Newtonian fluid (in accordance with predictions by Jeffery [12]) and by Słowicka et al. [20] for a single (but generally shorter) fibre in a Newtonian Poiseuille flow. However, let us first note that the

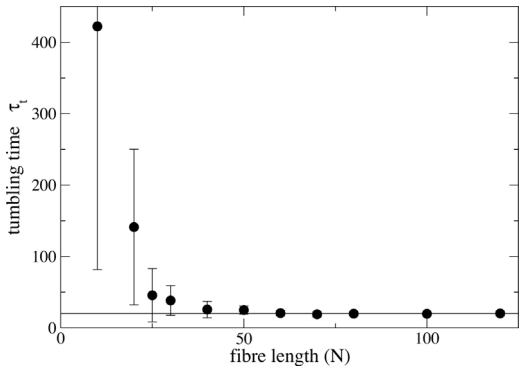

Fig. 7. Dimensionless tumbling time $\tau_t = \dot{\gamma} T_t$ as a function of the length N of the fibre, for $De = 1.0 \times 10^{-3}$ and stiffness $S = 1.0$. Vertical bars represent standard deviation of successive tumbling times. The straight line is the period $\tau_0 = 20$.

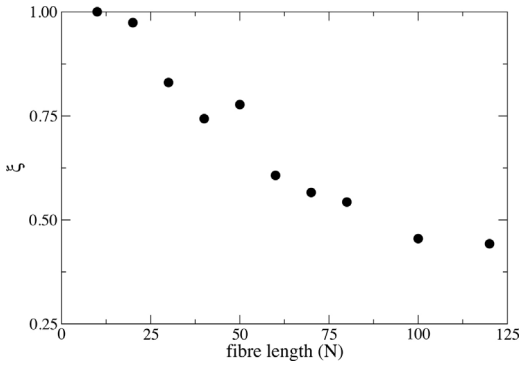

Fig. 8. Fraction of the time, ξ, that the fibre spends in a relatively straight configuration ($\alpha < 0.2$), as a function of its length N ($S = 1.0$ and $De = 1.0 \times 10^{-3}$ as in Fig. 7). Longer fibres tend to spend more time in a coiled configuration while flipping.

tumbling time quickly reaches a steady value $\tau_0 \simeq 20$ when the fibre length exceeds 50 particles. Furthermore, very short fibres tend to exhibit chaotic dynamics with scarce random flips, which results in a very large dispersion in measured tumbling times (see error bars in Fig. 7).

Let us insist on the fact that even if the tumbling time becomes independent of the fibre length, the detailed dynamics of the fibre can still differ. This can be evidenced by plotting the fraction of time ξ that the fibre spends in a roughly straight geometry, defined as $\alpha < 0.2$ (i.e., a configuration is considered as straight if $L/L_0 > 0.8$). As illustrated in Fig. 8, ξ is equal to 1 for very short fibres (which behave like rigid elongated particles) and continuously decreases with increasing fibre length. If, for short fibres, the flipping transition is almost instantaneous compared to the tumbling time, these two times become of the same order as the fibre gets longer, until the latter spends most of the time in a relatively coiled geometry.

In Fig. 9, we plot the orbits described by the two ends of the fibre in time, normalized by their distance at equilibrium. The orbit is close to a circle for the shortest fibre, which behaves like a rigid object. It is then quickly flattened in the transverse direction when the fibre gets longer. Let us remark, however, that in this case the streamwise distance between the two ends of the fibre does not represent the maximum streamwise extension of the fibre.

3.4. Influence of fibre stiffness

In Fig. 10 we plot the variation of tumbling time as a function of the dimensionless stiffness of a fibre made of $N = 50$ particles, for $S = 0.02$ to $S = 35$. Considering the dispersion in observed tumbling times, we can conclude that in the range that we consider here, the stiffness of the fibre does not affect the tumbling time. This is

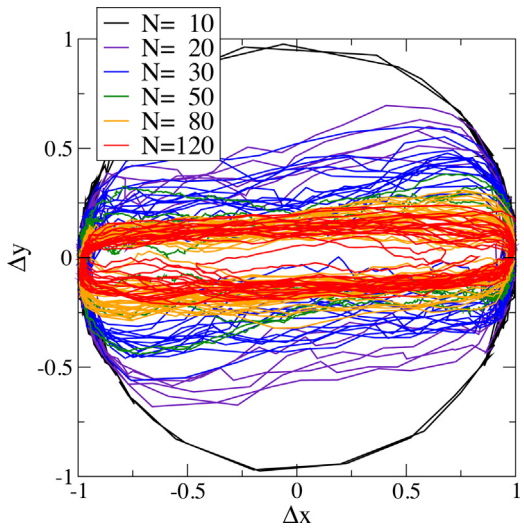

Fig. 9. Transverse component versus streamwise component of the fibre end-to-end vector for different lengths of the fibre, each component being normalized by the fibre length N. The longer the fibre, the flatter is the orbit.

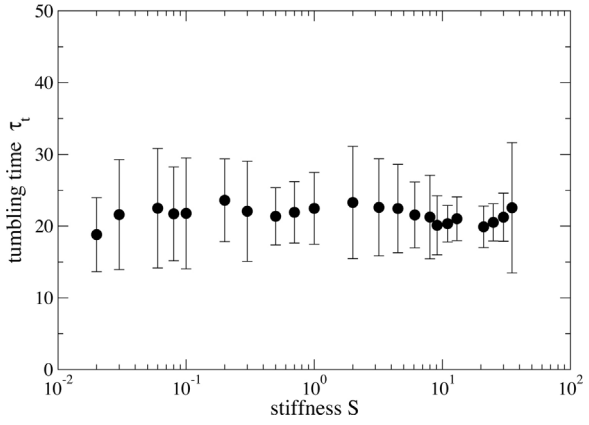

Fig. 10. Tumbling time as a function of the dimensionless stiffness of the fibre, for a length $N = 50$ and Deborah number $De = 10^{-3}$. Within the considered range, the tumbling time can be considered as independent of the fibre stiffness.

partially consistent with the results of Yamamoto and Matsuoka [28] which show that the tumbling time in a Newtonian fluid becomes constant if the fibre is rigid enough. As in the case of the influence of the fibre length, it is striking that the tumbling time remains almost invariant although the detailed dynamics of the flipping motion is different, as illustrated by Fig. 11 where we plot the standard deviation of the normalized transverse span of the fibre $\Delta y/L_0$. As can be seen, the average transverse extension of the fibre during the tumbling motion increases with its stiffness: flexible fibres are able to flip by taking sinuous shapes (which was called 'snake turn' by Forgacs and Mason [8]), while stiffer fibres can only flip like rigid rods. In all cases, natural transverse velocity fluctuations of the bubbles constantly disturb the fibre from its straightened position aligned with the flow, which results in some parts of the fibre being accelerated. In the flexible case, as shown in Fig. 11, the typical transverse span is of the order of $\Delta y \sim L_0/10$. This implies that the relative velocity of both ends of the fibre is of the order of $\Delta v \sim \dot{\gamma} \times L_0/10$. In order to flip, the fastest end of the fibre needs to be displaced by a distance $2L_0$, which leads to a normalized tumbling time

$$\tau_t = \dot{\gamma} T_t = \dot{\gamma} \times \frac{2L_0}{\Delta v} \sim 20\,, \tag{10}$$

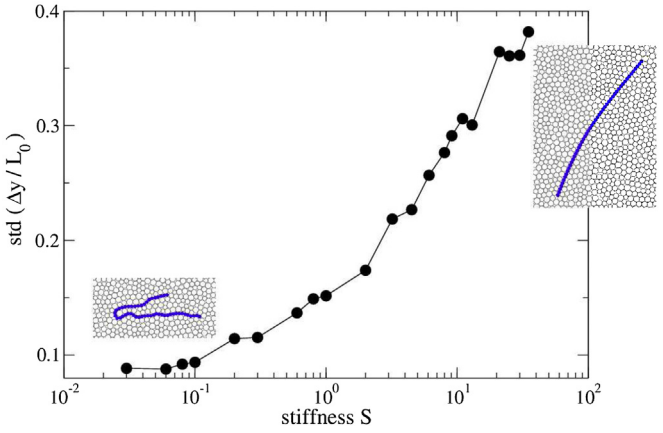

Fig. 11. Standard deviation of the transverse span $\Delta y(t)$ of the fibre, normalized by the equilibrium length L_0, as a function of the stiffness S. Snapshots show the typical shape of the fibre during a flip in the limits $S \sim 0.1$ and $S \sim 20$.

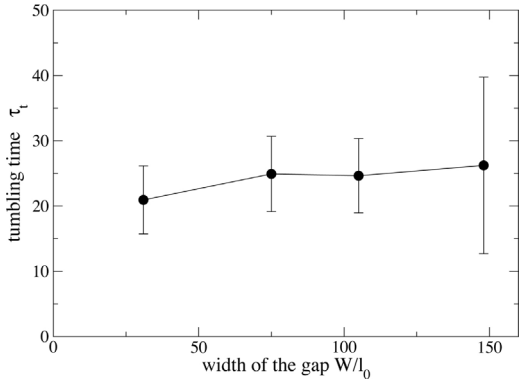

Fig. 12. Dimensionless tumbling time $\tau_t = \dot{\gamma} T_t$ as a function of the width of the gap, normalized by the equilibrium length of the fibre l_0. Vertical bars represent standard deviation of successive tumbling times. We cannot conclude any particular influence of the gap width on the tumbling time.

consistent with our observations (Figs. 6 and 10). In the rigid limit, the ends of the fibre undergo roughly circular orbits. In a Newtonian fluid, the tumbling time should be equal to half the period predicted by Jeffery [12] for rigid ellipsoids of aspect ratio r: $\tau_J = \pi \times \left(r + 1/r\right)$. Extrapolating the effective aspect ratio r^* of a cylindrical rods that behaves like an ellipsoidal rod of aspect ratio r [4,28], we find $r^* = 35$ for a fibre of length $N = 50$, which corresponds to $\tau_J = 110 \gg \tau_0$. Hence the actual tumbling time that we observe in our simulations is much shorter than predicted in a Newtonian fluid by Jeffery.

3.5. Influence of gap width

Finally, we varied the width of the gap between the two sidewalls, and plotted the average tumbling time in Fig. 12. Let us note that the very large dispersion for the widest gap is in fact due to a small number of abnormally long times without any flip. However, considering the dispersion, it is difficult to assess that the width of the gap has any major influence on the tumbling time. Interestingly, it is also observed that the tumbling motion still occurs even when the width of the gap is smaller than the length of the fibre (if the latter is sufficiently flexible).

4. Conclusion

In this article we have presented the first model of a fibre-laden foam. By combining the bubble model used in foam physics with a particulate model of a fibre classically used in simulations of fibre suspensions, we have investigated the dynamics of an individual flexible fibre within the shear flow of a 2D foam. Our simulations show that the tumbling time decreases as a power law of the strain rate, close to the inverse relationship already observed for fibres in a Newtonian shear flow. We also observe that the tumbling motion gets faster when the fibre gets longer, but becomes constant when the fibre length exceeds 50 bubble diameters. Interestingly, the tumbling time is also observed to be constant (with $\dot{\gamma} T_t \simeq 20$) when fibre stiffness is increased over 3 decades, though the detailed dynamics of the flipping motion is qualitatively different: short and rigid fibres describe roughly circular orbits and remain straightened, while long and flexible fibres spend most of the time in a coiled geometry and become sinuous when flipping. These results imply that using foam as a carrier fluid is not enough to keep fibres aligned in the direction of the flow. With this same issue in mind, we shall address the dynamics and interactions of multiple fibres in suspension within a foam, and the rheology of such a three-phase fluid, in a further article.

Recent experimental studies [3] suggest that the rheology of a fibre-laden foam can be affected by the surface properties of the fibres (which can be either smooth or rough). This effect could readily be incorporated in our model by adding a tunable attractive force between the fibre particles and adjacent bubbles, and between different fibres. Performing 2D experiments with model fibres in well-controlled flows would be useful to help tuning these numerical ingredients. Finally, let us note that the model can also conveniently be extended to non-homogeneous strain rates (e.g. for a pipe flow) and, by adding twisting forces, to a suspension of fibres in a 3D foam.

Acknowledgments

This work has emanated from research supported in part by a research grant from Science Foundation Ireland (SFI) under grant number 13/IA/1926. This article is based upon work from COST Actions MP1106 'Smart and green interfaces' and MP1305 'Flowing matter', supported by COST (European Cooperation in Science and Technology). We also acknowledge the support of the European Space Agency ESA, Project microG-Foam, AO-99-075 and contract 4000115113, 'Soft Matter Dynamics'. We would like to thank F. Dunne for stimulating discussions.

References

[1] A.M. Al-Qararah, A. Ekman, T. Hjelt, J.A. Ketoja, H. Kiiskinen, A. Koponen, J. Timonen, A unique microstructure of the fiber networks deposited from foam-fiber suspensions, Colloids Surf. A: Physicochem. Eng. Aspects 482 (2015) 544–553, http://dx.doi.org/10.1016/j.colsurfa.2015.07.010.
[2] A.M. Al-Qararah, T. Hjelt, A. Koponen, A. Harlin, J.A. Ketoja, Bubble size and air content of wet fibre foams in axial mixing with macro-instabilities, Colloids Surf. A: Physicochem. Eng. Aspects 436 (2013) 1130–1139, http://dx.doi.org/10.1016/j.colsurfa.2013.08.051.
[3] A.M. Al-Qararah, T. Hjelt, A. Koponen, A. Harlin, J.A. Ketoja, Response of wet foam to fibre mixing, Colloids Surf. A: Physicochem. Eng. Aspects 467 (2015) 97–106, http://dx.doi.org/10.1016/j.colsurfa.2014.11.034.
[4] F.P. Bretherton, The motion of rigid particles in a shear flow at low Reynolds number, J. Fluid Mech. 14 (1962) 284–304.
[5] I. Cantat, S. Cohen-Addad, F. Elias, F. Graner, R. Höhler, O. Pitois, F. Rouyer, A. Saint-Jalmes, Foams: Structure and Dynamics, OUP, Oxford, 2013.
[6] D. Durian, Foam mechanics at the bubble scale, Phys. Rev. Lett. 75 (1995) 4780–4783, http://dx.doi.org/10.1103/PhysRevLett.75.4780.
[7] A. Farutin, T. Piasecki, A.M. Słowicka, C. Misbah, E. Wajnryb, M.L. Ekiel-Jezewska, Dynamics of flexible fibers and vesicles in Poiseuille flow at low Reynolds number, Soft Matter 42 (2016) 7307–7323, http://dx.doi.org/10.1039/C6SM00819D.
[8] O. Forgacs, S. Mason, Particle motions in sheared suspensions: IX. Spin and deformation of threadlike particles, J. Colloid Sci. 14 (1959) 457–472.
[9] E. Gauger, H. Stark, Numerical study of a microscopic artificial swimmer, Phys. Rev. E 74 (2006) 021907, http://dx.doi.org/10.1103/PhysRevE.74.021907.

[10] B. Haffner, F.F. Dunne, S.R. Burke, S. Hutzler, Ageing of fibre-laden aqueous foams, Cellulose 24 (2017) 231–239, http://dx.doi.org/10.1007/s10570-016-1100-1.
[11] A. Jäsberg, P. Selenius, A. Koponen, Experimental results on the flow rheology of fiber-laden aqueous foams, Colloids Surf. A: Physicochem. Eng. Aspects 473 (2015) 147–155, http://dx.doi.org/10.1016/j.colsurfa.2014.11.041.
[12] G.B. Jeffery, The motion of ellipsoidal particles immersed in a viscous fluid, in: Proc. R. Soc. Lond. A: Math. Phys. Eng. Sci., 1922, pp. 161–217.
[13] V.J. Langlois, The two-dimensional flow of a foam through a constriction: insights from the bubble model, J. Rheol. 58 (2014) 799–818, http://dx.doi.org/10.1122/1.4872058.
[14] V.J. Langlois, S. Hutzler, D. Weaire, Rheological properties of the soft-disk model of two-dimensional foams, Phys. Rev. E 78 (2008) 021401, http://dx.doi.org/10.1103/PhysRevE.78.021401.
[15] A. Lindner, M. Shelley, Elastic Fibers in Flows, Royal Society of Chemistry, Cambridge, UK, 2015, 168 p.
[16] S.B. Lindström, T. Uesaka, Simulation of the motion of flexible fibers in viscous fluid flow, Phys. Fluids 19 (2007) 0–16, http://dx.doi.org/10.1063/1.2778937.
[17] T. Pöschel, T. Schwager, Computational Granular Dynamics: Models and Algorithms, Springer-Verlag, Berlin, 2005.
[18] R.F. Ross, D.J. Klingenberg, Dynamic simulation of flexible fibers composed of linked rigid bodies, J. Chem. Phys. 106 (1997) 2949–2960, http://dx.doi.org/10.1063/1.473067.
[19] M.B. Sexton, M.E. Möbius, S. Hutzler, Bubble dynamics and rheology in sheared two-dimensional foams, Soft Matter 7 (2011) 11252–11258, http://dx.doi.org/10.1039/C1SM06445B.
[20] A.M. Słowicka, M.L. Ekiel-Jezewska, K. Sadlej, E. Wajnryb, Dynamics of fibers in a wide microchannel, J. Chem. Phys. 136 (2012) 0–8, http://dx.doi.org/10.1063/1.3678852.
[21] A.M. Słowicka, E. Wajnryb, M.L. Ekiel-Jezewska, Dynamics of flexible fibers in shear flow, J. Chem. Phys. 143 (2015) 124904, http://dx.doi.org/10.1063/1.4931598.
[22] M. Smith, V. Punton, A. Rixson, Structure and properties of paper formed by a foaming process, Tappi 57 (1974) 107–111.
[23] G. Subramanian, D.L. Koch, Inertial effects on fibre motion in simple shear flow, J. Fluid Mech. 535 (2005) 383–414, http://dx.doi.org/10.1017/S0022112005004829.
[24] L.H. Switzer, D.J. Klingenberg, Rheology of sheared flexible fiber suspensions via fiber-level simulations, J. Rheol. 47 (2003) 759, http://dx.doi.org/10.1122/1.1566034.
[25] E. Wandersman, N. Quennouz, M. Fermigier, A. Lindner, O. Du Roure, Buckled in translation, Soft Matter 6 (2010) 5715–5719, http://dx.doi.org/10.1039/C0SM00132E.
[26] D. Weaire, S. Hutzler, The Physics of Foams, Oxford University Press, Oxford, 1999.
[27] D. Whyte, B. Haffner, A. Tanaka, T. Hjelt, S. Hutzler, The Interactions of fibres with soap films, Colloids Surf. A 534 (2017) 112–119, http://dx.doi.org/10.1016/j.colsurfa.2017.02.037.
[28] S. Yamamoto, T. Matsuoka, A method for dynamic simulation of rigid and flexible fibers in a flow field, J. Chem. Phys. 98 (1993) 644–650, http://dx.doi.org/10.1063/1.464607.
[29] S. Yamamoto, T. Matsuoka, Dynamic simulation of microstructure and rheology of fiber suspensions, Polym. Eng. Sci. 36 (1996) 2396–2403, http://dx.doi.org/10.1002/pen.10638.